ORIGINAL RESEARCH

Spontaneous rearrangement of acetylated xylan on hydrophilic cellulose surfaces

Madhulika Gupta · Takat B. Rawal · Paul Dupree · Jeremy C. Smith · Loukas Petridis

Abstract The interaction of xylan, an abundant plant polysaccharide, with cellulose microfibrils is essential for secondary cell wall strength. A deeper understanding of these interactions is crucial both to improve our understanding of plant cell wall architecture and to design alternate strategies to overcome cellulose recalcitrance for the production of biofuels and sustainable biomaterials. Naturally occurring acetate or glucuronic acid substitutions on xylan have been shown to influence xylan-cellulose interactions. Here, we use unrestrained molecular dynamics simulations to determine the interactions with the (110) hydrophilic face of cellulose fibers of four different xylans. In the absence of cellulose, all xylans, independent of the substitution pattern, adopt a highly flexible threefold helical screw conformation. However, when xylan is spatially close to a cellulose surface 1,2 linked acetyl xylans (2AcX) adopt rigid twofold helical screw conformations. The 2AcX conformations are primarily stabilized by interactions between the acetylated oxygen and the glycosidic linkage with C-O6 of cellulose. In contrast, the glycosidic oxygens and acetyl decorations for 1,3 linked acetyl groups (3AcX) are oriented away from the cellulose surface and the 3AcX xylans maintain threefold helical screw conformations on the cellulose surface. Our results show that evenly spaced chemical functionalization (with acetyl groups) and the position of substitution (1,2) on xylan backbone play key roles in tuning the xylan-cellulose interactions to stabilize the twofold helical screw conformations of xylan on the cellulose surface. A comparison with previous experimental findings further suggests that 1,2 substitutions induce twofold helical screw conformations of xylan on the cellulose surface irrespective of the chemical nature of the substituent, while 1,3 substitutions primarily bind lignin in threefold helical screw conformations rather than cellulose in plant cell walls.

M. Gupta · J. C. Smith · L. Petridis (✉)
Oak Ridge National Laboratory, UT/ORNL Center for Molecular Biophysics, Oak Ridge, TN 37831, USA
e-mail: petridisl@ornl.gov

M. Gupta
VIT Bhopal University, Kotri Kalan, Sehore, Madhya Pradesh 466114, India

T. B. Rawal · J. C. Smith · L. Petridis
Department of Biochemistry and Cellular and Molecular Biology, University of Tennessee, Knoxville, TN 37996, USA

P. Dupree
Department of Biochemistry and Leverhulme Centre for Natural Material Innovation, University of Cambridge, Cambridge CB2 1QW, UK

Introduction

Plant cell walls are complex composite biomaterials
mostly comprising cellulose, hemicellulose, lignin,
and pectins. These renewable biopolymers are abun-
dant and promising resources for the sustainable
production of green biomaterials and biofuels (Pauly
and Keegstra 2010; Rijn et al. 2018). The structural
and mechanical properties of plant cell walls are
governed at the molecular level primarily by the
interactions of hemicellulose, lignin and cellulose.
Hemicelluloses interact with both cellulose and lignin
to form a strong composite material (Tarasov et al.
2018). In particular, the interactions between hemi-
cellulose and cellulose affect the strength and rigidity
of the cell walls while also impeding cellulose
conversion to biofuels (Cosgrove and Jarvis 2012;
Kumar et al. 2018). To fully realize the potential of
biomass as a renewable resource and to refine the
existing models of the architecture of cell walls, an
improved understanding of these molecular level
interactions is essential (Himmel et al. 2007; Carroll
and Somerville 2009; Pauly and Keegstra 2010;
Chundawat et al. 2011; Meng and Ragauskas 2014).

In plants, celluloses are found in the form of
partially crystalline microfibrils that are composed of
18 glucan chains (Kubicki et al. 2018; Song et al.
2020), which interact via lateral hydrogen bonding and
adopt twofold helical screw conformations (one 360°
twist per two glycosidic bonds) (French and Johnson
2009). This arrangement is driven by a complex
network of intra- and inter-molecular hydrogen bonds
(Nishiyama et al. 2002). Xylan is a prominent type of
hemicellulose that is found in hardwood, grass cell
walls, eudicot secondary cell walls, and conifer walls
(Ebringerova and Heinze 2000; Scheller and Ulvskov
2010). It is a linear polymer of β-1,4-linked D-xylosyl
units. The xylan backbone is ubiquitously decorated
by different side-chain substitutions in plants. Some of
the common substitutions are α-1,2-(4-*O*-methyl)
D-glucuronic acid (MeGlcA), α-1,2 or α-1,3-L-arabi-
nofuranosyl (Ara) and acetyl (Ac) side chains
(Ebringerova and Heinze 2000; de Carvalho et al.

2019; Lunin et al. 2020). These substitutions facilitate
cellulose-xylan interactions and are essential in main-
taining the function and solubility of xylan chains as
well as preventing enzymatic digestion by microbes
and parasitic attacks (Biely and Mackenzie 1986;
Mortimer et al. 2010; Xiong et al. 2013, 2015;
Mikkelsen et al. 2015). In addition to xylan type, pH
and temperature also affect xylan-cellulose interac-
tions (Westbye et al. 2006; Busse-Wicher et al. 2014;
Kumar et al. 2018).

The substitutions on the xylan backbone are not
random but follow a pattern where usually every even
xylosyl residue is substituted (Bromley et al. 2013;
Busse-Wicher et al. 2014, 2016; Martínez-Abad et al.
2017). Solid-state nuclear magnetic resonance
(ssNMR) shows that even substitutions are essential
for normal interaction with cellulose microfibrils and
are a highly conserved feature in all vascular plants
(Busse-Wicher et al. 2016; Grantham et al. 2017). The
pattern of substitution and the chemical nature of the
substituents vary depending on the plant taxonomic
family and type of cell wall (Ebringerova and Heinze
2000; Scheller and Ulvskov 2010; Koutaniemi et al.
2012). Xylan is usually decorated with Ara and
MeGlcA in gymnosperms, while Ac substitutions are
found in gnetophytes, monocots, eudicots, and early
diverging angiosperms like magnolia (Ebringerova
and Heinze 2000; Busse-Wicher et al. 2016). The
presence of Ac groups is essential to maintain
solubility of the xylan chain and prevent it from
precipitation (Mortimer et al. 2010). The degree of
acetylation as well as the position of these substitu-
tions play a key role in determining the hydrophobic-
ity, and hence the rigidity, of the plant cell wall which
is vital for the xylan function (Teleman et al. 2002;
Qaseem and Wu 2020). The exact degree of acetyla-
tion is not yet known but previous studies have shown
that it can be as high as 0.7 in hardwood xylans (Pawar
et al. 2013) with an average of 0.06 in Poplar (Johnson
et al. 2017). In eudicots such as *Arabidopsis,* about
50% of the xylosyl residues are acetylated with every
even residue bearing the acetylation at O-2 or O-3 or
both positions (Evtuguin et al. 2003; Xiong et al. 2013;
Busse-Wicher et al. 2014). Substitution also affects
xylan adsorption onto cellulose (Mortimer et al. 2010;
Xiong et al. 2013, 2015; Falcoz-Vigne et al. 2017;
Jaafar et al. 2019) with α-1,2 GlcA decorated xylan in
Arabidopsis being more difficult to extract than the
xylan without α-1,2 GlcA, suggesting altered

interactions with other cell wall polymers (Mortimer et al. 2010). Strong reduction in xylan acetylation results in structural abnormalities, dwarfism, and reduced mechanical strength of plant cell walls (Bischoff et al. 2010; Xiong et al. 2013; Gao et al. 2017; Zhang et al. 2017), thus emphasizing the importance of acetylation in the plant cell walls.

In the absence of cellulose, xylan is flexible and forms threefold helical screw conformations (one 360° twist per three glycosidic bonds) in water (Nieduszynski and Marchessault 1972; Almond and Sheenan 2003; Busse-Wicher et al. 2014; Falcoz-Vigne et al. 2017). ssNMR studies of *Arabidopsis* stems (Simmons et al. 2016) and birch pulp (Falcoz-Vigne et al. 2017) along with molecular dynamics (MD) simulations (Busse-Wicher et al. 2014, 2016) found that xylan flattens into a ribbon-like twofold helical screw when interacting with the cellulose surface, with the twofold screw xylan having similar rigidity to cellulose microfibrils (Simmons et al. 2016). A combination of quartz crystal microbalance with dissipation (QCM-D) and MD studies has been used to establish that the change in xylan conformation is influenced by its interactions with cellulose and that Ac substitutions play a key role in mediating cellulose-xylan interactions (Jaafar et al. 2019). Per-acetylated xylan at both O-2 and O-3 positions adopt twofold conformations on (110), (1–10) and (100) cellulose surfaces, while for deacetylated xylan, these conformations are retained only by the xylan chain which was in direct contact with the cellulose surface. Re-adsorption studies further showed that only the xylan chain which is in direct contact with the cellulose surface adopts twofold conformations, while subsequent layers of xylan are mostly present in threefold conformations (Falcoz-Vigne et al. 2017). The unsubstituted face of the xylan backbone forms hydrogen bonds with the cellulose surface while the substituted residues point away from the cellulose surface (Busse-Wicher et al. 2014, 2016).

Recently, ssNMR studies of maize cell walls suggested that xylan has a dual function, with one-third of xylan conformations being threefold and binding lignin via xylan-aromatic interactions, while the twofold xylan conformations bind cellulose (Kang et al. 2019). The energy difference between the threefold and twofold helical screw conformations of xylan is relatively low and thus, these structures can interconvert depending on the absence or presence of

cellulose (Berglund et al. 2016; Ling et al. 2020). Xylans therefore play a significant role in bridging cellulose and lignin in plant cell walls by adopting diverse conformational structures.

In contrast to xylans, cellulose maintains a rigid twofold helical screw conformation. The major difference between xylan and cellulose is the presence of an exocyclic CH_2OH group in cellulose. Recent DFT studies on the disaccharides of cellulose and xylan (cellobiose and xylobiose, respectively) highlight the importance of the C6 moiety in stabilizing the twofold helical screw conformations in cellulose (Ling et al. 2020). These studies showed that the presence of the C6 moiety in cellulose restricts the glycosidic dihedral angles in regions where the intra-molecular hydrogen bonds are more likely. In contrast, the glycosidic dihedral angles in xylan occupy broader conformational space and lack intra-molecular hydrogen bonds, rendering it more flexible. Thus, the presence of the C6 group has a considerable influence on the formation of twofold helical screw conformations in cellulose, as was also shown in a previous MD study (Pereira et al. 2017).

α-1,2 (or O-2) substitutions by Ara/MeGlcA groups in *Arabidopsis* reduce the conformational fluctuations of the xylan backbone, promoting interactions with the hydrophilic face of cellulose (Pereira et al. 2017; Shrestha et al. 2019). In contrast, α-1,3 (or O-3) Ara substitutions are involved in other functions in plant cell walls rather than stabilizing xylan-cellulose interactions (Pereira et al. 2017). These studies show that α-1,2 and α-1,3 Ara/GlcA substitutions influence cellulose-xylan interactions. However, the roles of other common xylan substituents, such as Ac groups, have not been yet fully investigated. Another recent study has shown that mannans are more flexible when acetylated at O-3, while acetylation at O-2 positions restricts the glycosidic dihedral angles due to steric hindrance of axial positions resulting in the formation of more rigid twofold helical screw conformations on the cellulose surface (Berglund et al. 2020).

To understand the effects of Ac and MeGlcA xylan decorations on its association with cellulose and to reveal the interactions that stabilize the twofold helical screw xylan conformations, we performed unrestrained MD simulations of four solvated xylans both in the absence and presence of cellulose (Fig. 1). We constructed O-2 and O-3 decorated xylan models (Fig. 2) with degree of polymerization DP = 11,

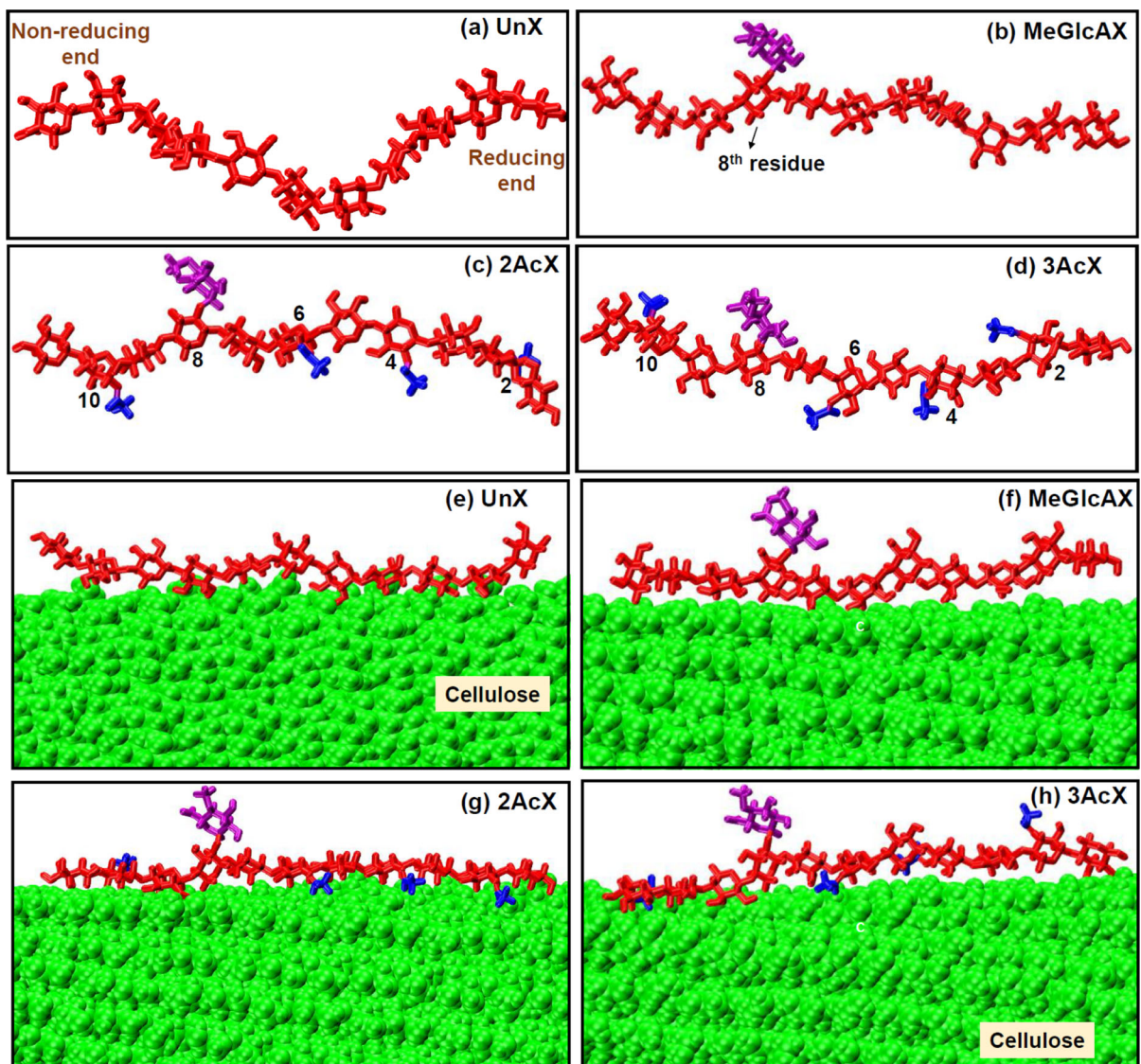**Fig. 1** Representative snapshots of xylan decorations in (**a**–**d**) water, and (**e**–**h**) presence of cellulose. The xylan backbone is shown in red, while MeGlcA and Ac decorations are shown in purple and blue, respectively. Cellulose is shown in green. The xylans are placed on (110) hydrophilic face of cellulose

denoted as 2AcX and 3AcX, respectively. In 2AcX and 3AcX, every alternate residue on the xylan backbone is substituted to match the even pattern of substitutions on xylan in experimental findings (Brown et al. 2007; Bromley et al. 2013; Busse-Wicher et al. 2014, 2016). There has been substantial evidence about the presence of MeGlcA substitution on every 8th residue in the cell walls of *Arabidopsis* stems (Brown et al. 2007). To take this into account, the Ac substitutions were performed on residues 2, 4,

6, and 10 and MeGlcA substitution on residue 8. As controls, we also constructed a xylan backbone with only one substitution by MeGlcA group on the 8th residue, denoted as MeGlcAX, and a bare xylan backbone which has no substitutions at all and is denoted as UnX. The binding of xylan on the hydrophobic cellulose surface is influenced by hydrophobic interactions whereas hydrogen bonding interactions dominate on the hydrophilic cellulose surface (Busse-Wicher et al. 2014, 2016; Falcoz-

Vigne et al. 2017; Martínez-Abad et al. 2017). These studies also showed that the presence of substitutions plays a particularly important role in stabilizing cellulose-xylan interactions on the hydrophilic cellulose surface. Thus, the choice of the cellulose surface influences the interactions between the xylan backbone and cellulose microfibrils. Previous MD studies support the stable binding of twofold helical screw conformations of xylan decorations on the more exposed (110) hydrophilic face of cellulose (Busse-Wicher et al. 2016) despite the lack of grooves on this surface and have examined the effect of α-1,2 and α-1,3 Ara and GlcA xylan substitutions on this surface (Pereira et al. 2017). Thus, we choose the (110) hydrophilic surface for our simulations (Cosgrove 2014) to allow direct comparison with the previous MD work (Busse-Wicher et al. 2016; Pereira et al. 2017). NMR studies also support the strong binding of xylan to (110) hydrophilic surface rather than (1–10) surface (Larsson et al. 1999; Larsson 2003; Bergenstråhle et al. 2008).

The exact native compositions of cell walls are not known. Recent studies have shown that about 10% of the xylose units carry a MeGlcA unit in the O-2 position and are also acetylated at O-3 position in *Arabidopsis* while $\leq$ 6% of the xylose residues carry double acetylation at O-2 and O-3 positions (Busse-Wicher et al. 2014; Chong et al. 2014; Grantham et al. 2017). The simultaneous presence of MeGlcA at O-2 and Ac at O-3 is also seen for birch chips (Martínez-abad and Jiménez-quero 2020). Since only a small percentage of residues bear this double substitution by Ac or MeGlcA groups, we limit this study to consider only single substitutions on xylosyl residues. Moreover, it is not feasible to perform an Ac substitution for both 2AcX and 3AcX models at the MeGlcA substituted residue as the O-2 position is occupied by MeGlcA. The goal of this study is to investigate the importance of acetyl substitutions at O-2 and O-3 positions on xylan-cellulose interactions. Thus, we examine simplified mono-substituted xylosyl residues so as to not obscure any other effects and to maintain the total number of substitutions performed on the xylan backbone in 2AcX and 3AcX models.

We monitored which xylan decorations lead to a transition from a threefold to a twofold helical screw (Figs. 2e-f) when interacting with the (110) hydrophilic cellulose surface (Cosgrove 2014; Busse-Wicher et al. 2016). 2-Ac substitutions make hydrogen

bonds with the cellulose, triggering the transition from a flexible threefold to rigid twofold helical screw conformation. The residues around the single MeGlcA substitution adopt threefold conformations, even for O-2 Ac decorated xylan, which suggests that MeGlcA does not promote xylan-cellulose binding. In contrast to 2-Ac substituted xylan, 3-Ac substitutions show similar qualitative behavior with bare xylan, maintaining a threefold conformation and interacting weakly with cellulose. Our results are consistent with previous simulations, in which α-1,2 GlcA and Ara decorations on xylan enhanced the binding stability of single xylan chain with cellulose surface unlike α-1,3 substitutions (Pereira et al. 2017). However, the previously reported simulations for xylan in contact with the hydrophilic (010, 110) or the hydrophobic surface (200) surfaces were either partially restrained or docked to the cellulose surface in a twofold helical screw conformation (Busse-Wicher et al. 2014; Martínez-Abad et al. 2017; Pereira et al. 2017) and thus the interactions of xylan backbone with the cellulose surface could not be correlated to the changes in the helical screw of the conformations on the cellulose surface. (Fig. 3, 4, 5, 6, 7, 8).

Methods

Models. We constructed O-2 and O-3 Ac decorated xylan models with degree of polymerization DP = 11, denoted as 2AcX and 3AcX, respectively, with alternate backbone residues substituted to match experimental findings (Brown et al. 2007; Bromley et al. 2013; Busse-Wicher et al. 2014, 2016): Ac substitutions on residues 2, 4, 6, and 10 and MeGlcA substitution on residue 8. We also constructed a xylan backbone with only one substitution by MeGlcA group on the 8th residue, denoted as MeGlcAX, and a bare xylan backbone which has no substitutions at all and is denoted as UnX. The initial structures for UnX, MeGlcAX, 2AcX and 3AcX were built in CHARM-GUI (Jo et al. 2008, 2011; Park et al. 2017, 2019). The cellulose microfibril was modeled as half of a hexagonal 36-chain elementary fibril that was obtained using cellulose-builder (Gomes and Skaf 2012) using the Iβ polymorph (Nishiyama et al. 2002) with DP of 20. This model has both the (110) hydrophilic and (100) hydrophobic surfaces exposed (Thomas et al. 2013; Zhao et al. 2014). For this study, we use the
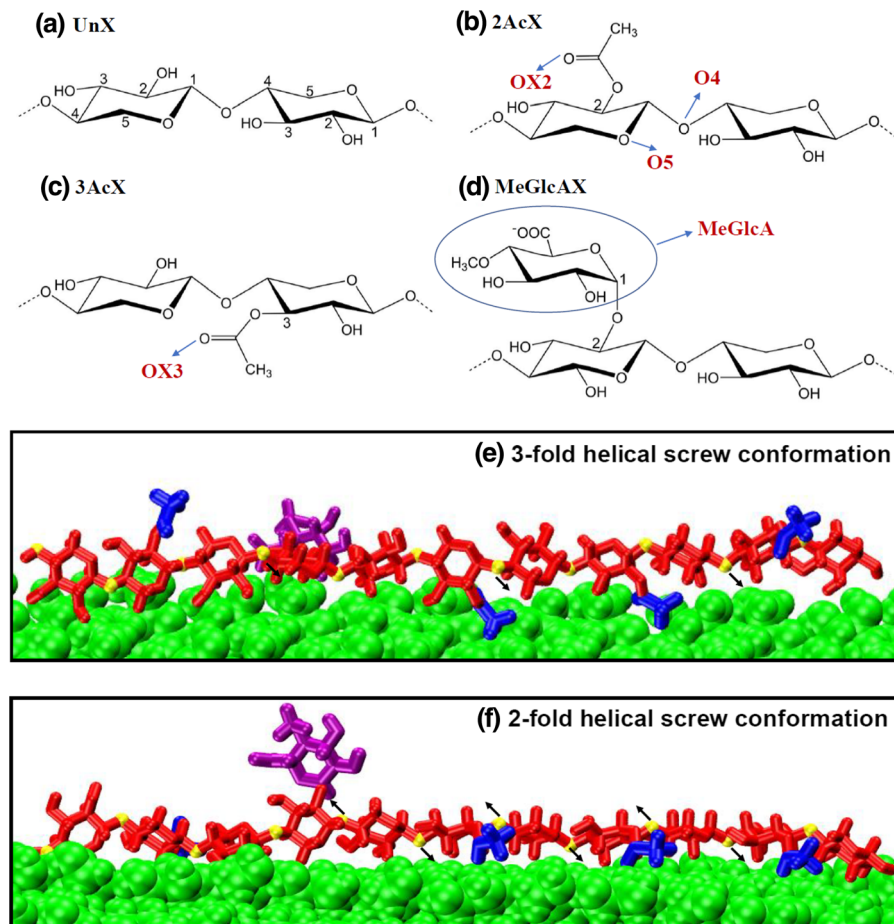
Fig. 2 (**a–d**) Chemical structures for different model systems. Representative snapshots for (**e**) threefold and (**f**) twofold helical screw conformations of xylan. The xylan backbone is shown in red, while MeGlcA and Ac decorations are shown in purple and blue colors, respectively. Cellulose is shown in green color

(110) hydrophilic surface of cellulose. Previous MD studies have been performed using xylan backbones of DPs ranging from 6–14 (Busse-Wicher et al. 2014, 2016; Falcoz-Vigne et al. 2017; Martínez-Abad et al. 2017; Pereira et al. 2017; Jaafar et al. 2019). These small xylan models (DP < 14) form good test systems for understanding the local conformations of xylan, such as the xylan folds studied here, particularly away from chain ends. However, the size of xylan chain may influence its interactions with the cellulose surface, since in general polymer solubility tends to decrease with DP.

MD simulations. Simulations were performed for the 4 xylan systems in the presence or in the absence of cellulose. All the systems were solvated with TIP3P water (Jorgensen et al. 1983) and the CHARMM force field for carbohydrates was used for all the simulations

(Guvench et al. 2009). An ionic strength of 0.15 M was maintained using KCl. All-atom MD simulations were performed with GROMACS (Abraham et al. 2015). All systems were first energy minimized followed by equilibration in the canonical NVT ensemble for 10 ns and 4 ns in the absence and presence of cellulose, respectively. Then isothermal-isobaric NPT equilibration was conducted for 50 ns and 4 ns in the absence and presence of cellulose, respectively. Position restraints were applied to non-hydrogen atoms of cellulose and xylan chains with a force constant of 1000 kcal mol^{-1} Å^{-2} during the equilibration runs. The temperature of 300 K was maintained during the simulations using the v-Rescale thermostat using a time constant of 1 ps (Bussi et al. 2007). The Parrinello-Rahman barostat (Parrinello and Rahman 1981) was used to maintain a pressure of
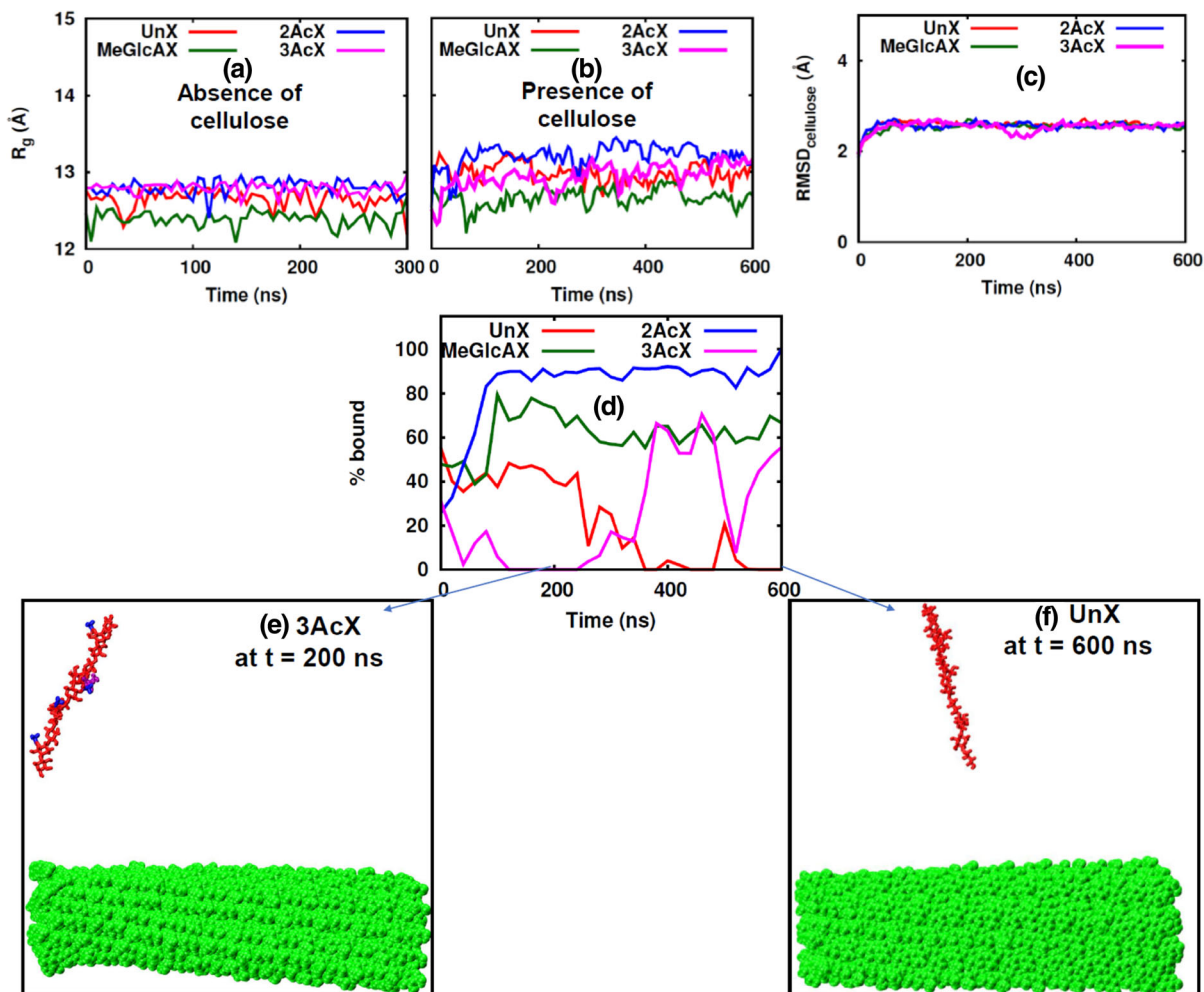
Fig. 3 Radius of gyration (R_g) as a function of time for xylan molecules in the (**a**) absence of cellulose, and (**b**) presence of cellulose. (**c**) Root mean square deviations (RMSD) of cellulose with respect to equilibrated restrained conformation. The data are averaged over four independent simulations for each system.

(**d**) Percentage of xylan conformations bound to (110) hydrophilic cellulose surface from a representative simulation run. Snapshots for desorbed xylan conformation for (**e**) 3AcX, and (**f**) UnX (color scheme same as Fig. 1

1 bar in NPT simulations with a relaxation time of 2 ps and an isothermal compressibility of 4.5×10^{-5} bar^{-1}. The cut-off used for van der Waals interactions was 12 Å with a switch distance of 10 Å. The electrostatic interactions were treated with the Particle Mesh Ewald (PME) method (Darden et al. 1993). The LINCS algorithm was used to constrain all bond lengths involving hydrogen atoms (Hess et al. 1997; Hess 2008). The leapfrog algorithm as implemented in GROMACS was used to integrate the equations of motion using an integration time step of 2 fs for all the simulations. The data were dumped every 50 ps.

For all four systems, sets of four independent simulations were performed. The initial configuration was used to perform four sets of minimization and equilibration runs independently, followed by unrestrained production runs, starting from different velocity distributions. In the absence of cellulose, the production runs were 300 ns each (1200 ns cumulative for each system), while in the presence of cellulose each production run was 600 ns (2400 ns cumulative for each system).

Analysis. The residues at the ends of the xylans were excluded from all the analyses. Data were averaged over four simulations for each system except
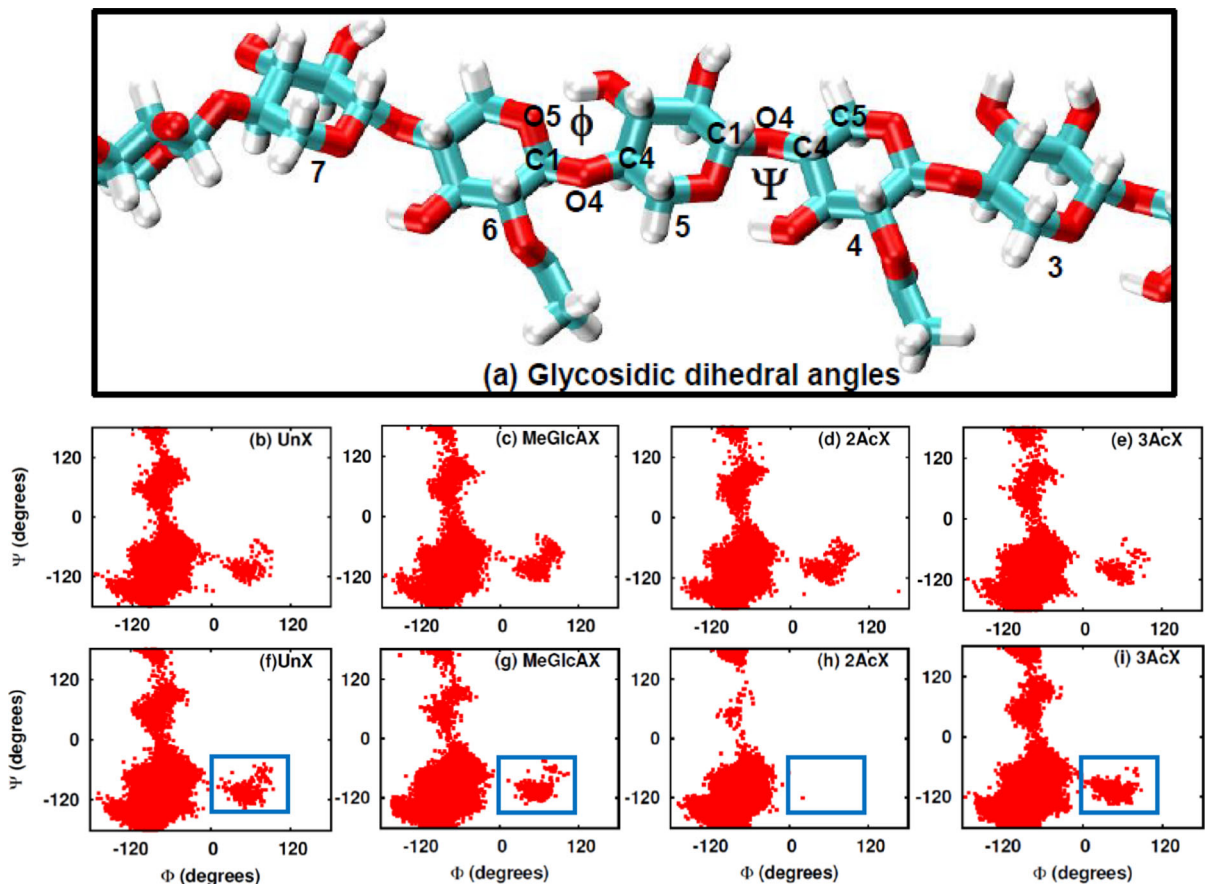
Fig. 4 **a** Representation of glycosidic dihedral angles. Distribution of glycosidic dihedral angles for xylans in **b–e** absence, and (**f-i**) presence of cellulose. The data is averaged over four independent simulations for each system
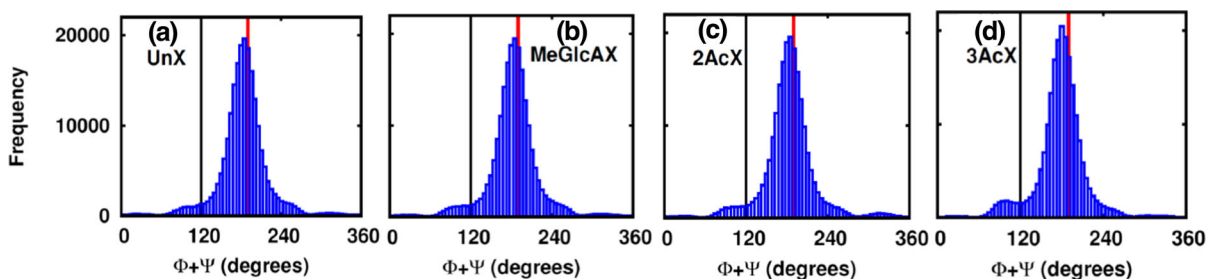

Fig. 5 Histograms for xylan conformations in the absence of cellulose. The black and red lines represent the sum of dihedral angles for twofold and threefold helical screw conformations, respectively. The data are averaged over all the residues in each of the four independent simulations for respective systems

for Figs. 9, 10, 11 that use individual simulations to determine the time regime at which xylan switches from threefold to twofold helical. The following residues of a particular system show similar qualitative behavior, and we only plot data for one of those residues: (a) residues 2–10 of UnX, (b) the unsubstituted residues 2–6 of MeGlcAX, (c) Ac substituted residues 2, 4 and 6 of 2AcX and 3AcX, (d) unsubstituted residues 3 and 5 of 2AcX and 3AcX.

The radius of gyration and root mean square deviations (RMSD) were computed using VMD (Humphrey et al. 1996), while all the other
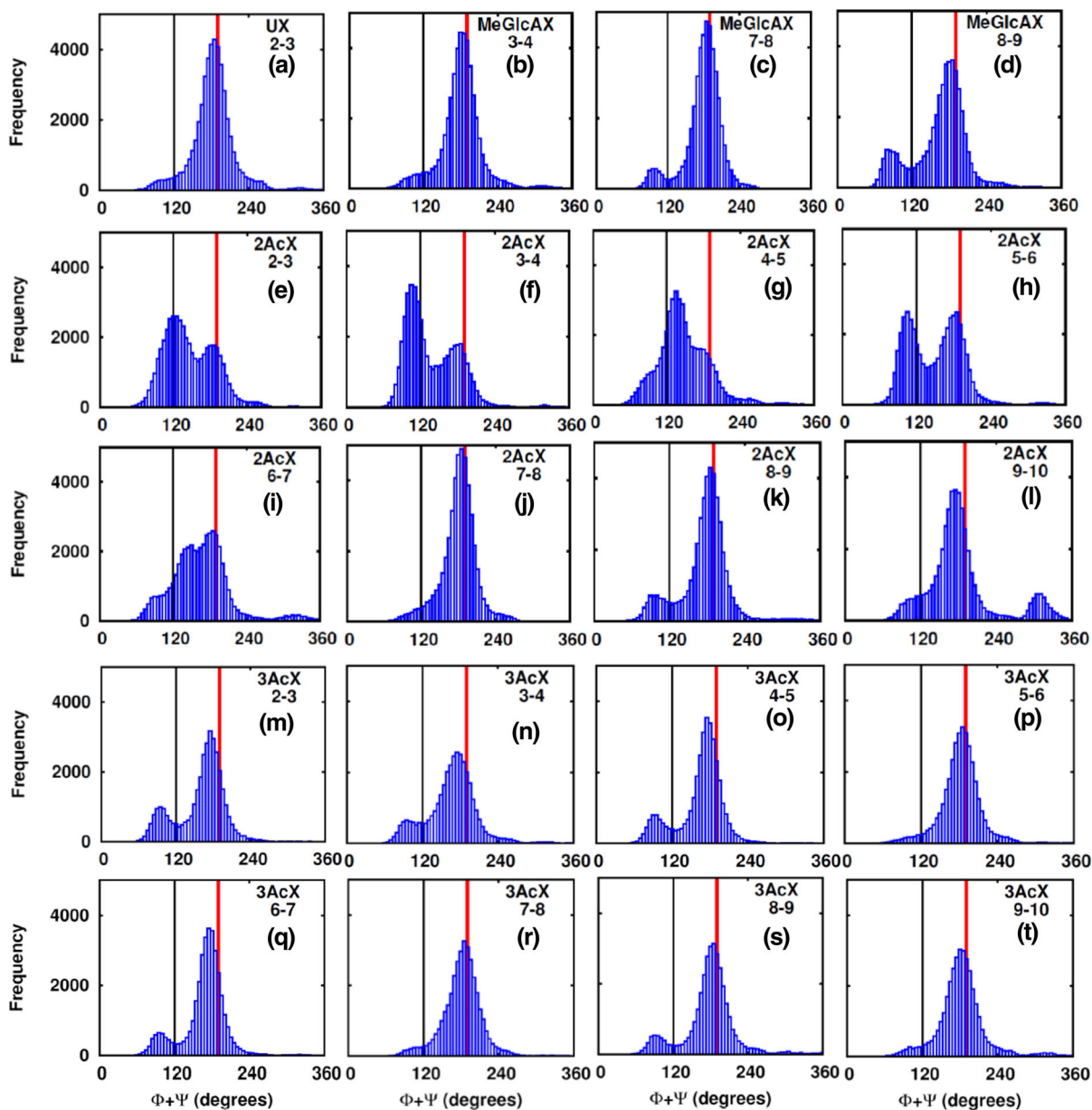
Fig. 6 Histograms for xylan conformations in the presence of cellulose for (**a**) UnX, (**b–d**) MeGlcAX, (**e–l**) 2AcX, and (**m–t**) 3AcX. The black and red lines represent the sum of dihedral angles for twofold and threefold helical screw conformations, respectively. The data are averaged over four independent simulations for respective systems

calculations were performed using GROMACS analysis tools (Abraham et al. 2015). A contact ($N_{contacts}$) is defined as formed when the distance of any atom of xylan to any atom of cellulose is ≤ 3.5 Å. A xylan conformation is defined as bound when each xylosyl residue form at least 15 contacts with the cellulose surface within a distance of 3.5 Å. A geometric definition of a hydrogen bond was used, with a donor–acceptor distance cut-off of 3.5 Å and H-donor–acceptor angle cutoff of 30°. We note that donor–acceptor distances are commonly employed to empirically define hydrogen bonds (Luzar 2000; Torshin et al. 2002). The averages and standard errors in different quantities are computed using the gmx
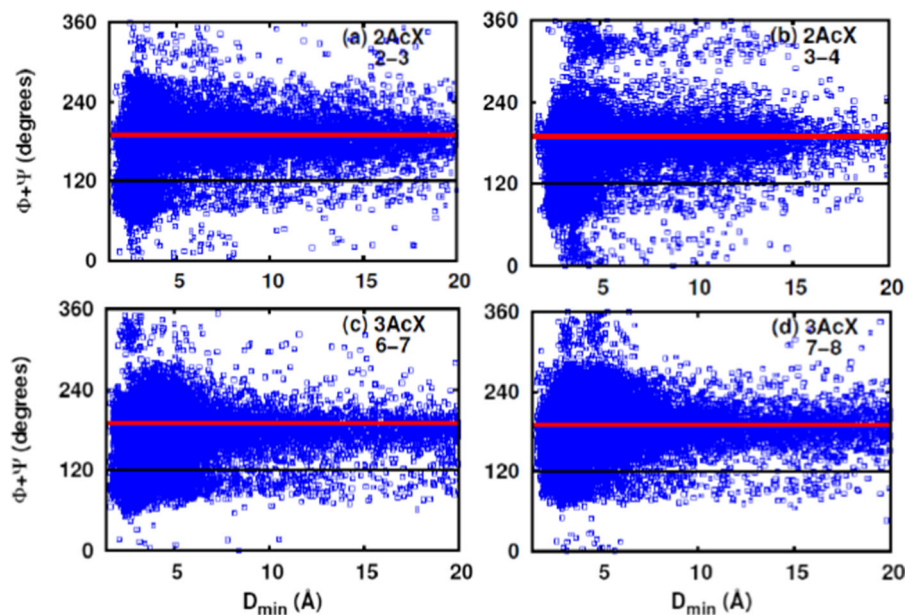
Fig. 7 Scatter plots showing distribution of glycosidic dihedral angles of xylan residues and their minimum distances from cellulose surface for (**a–b**) 2AcX, and (**c–d**) 3AcX. The black and red lines represent the sum of dihedral angles for twofold and threefold helical screw conformations, respectively

analyze tool which uses the standard error formula to calculate the standard errors in computed quantities. The standard error was computed from the time-averaged data over four independent simulations for each system.

Results and discussion

Xylan molecules were placed on top of the hydrophilic face (110) of cellulose, according to the crystalline arrangement (Fig. 1), and their 3D structure was compared to their unbound counterparts. This initial orientation of xylan on the surface of cellulose is one of many possibilities and a full exploration of multiple binding sites is beyond the scope of this work. In the absence of cellulose, the radius of gyration (R_g) of xylan shows similar fluctuations for all the four xylan systems both when xylan is unbound and when it is bound to the hydrophilic face of cellulose (Figs. 3a, 3b). Similarly, the root mean square fluctuations (RMSF) of the xylan show comparable behavior in the absence and presence of cellulose (Table 1). Despite a slight twist of the cellulose fiber (Busse-Wicher et al. 2014; Pereira et al. 2017), the cellulose RMSD is low (RMSD < 2.6 Å) for all systems

(Fig. 3c), indicating interactions with xylan do not distort the fiber. Interestingly, 2AcX and MeGlcAX remain bound to cellulose surface in all the four simulations. In one of the four simulations, UnX and 3AcX occasionally detach from the cellulose surface and diffuse into bulk (Fig. 3d). These detachment events suggest the importance of O-2 in stabilizing cellulose-xylan interactions in contrast to O-3 substituted xylan which shows similar behavior as that of bare xylan (Figs. 3e-f).

The glycosidic linkage dihedral angles, ϕ = C4(i)-O4(i)-C1($i + 1$)-O5($i + 1$), and Ψ = C5(i)-C4(i)-O4(i)-C1($i + 1$) between the ith and $(i + 1)^{th}$ residues characterize the local flexibility of the xylan backbone (Fig. 4a). In the absence of cellulose, UnX, 2AcX, and 3AcX show similar allowed values of dihedral angles, while the allowed dihedral range is more diverse for MeGlcAX (Fig. 4). In the presence of cellulose, the distributions of the dihedral angles for UnX and 3AcX are qualitatively similar to those in the cellulose-deficient environment and MeGlcAX has a slightly reduced dihedral range. 2AcX in the presence of cellulose shows a significant change, where the region $\phi > 0°$, $\Psi < 0°$ is not occupied at all by the 2AcX conformations in contrast to UX, MeGlcAX and 3AcX conformations (Figs. 4f-i). Thus, 2AcX has the most
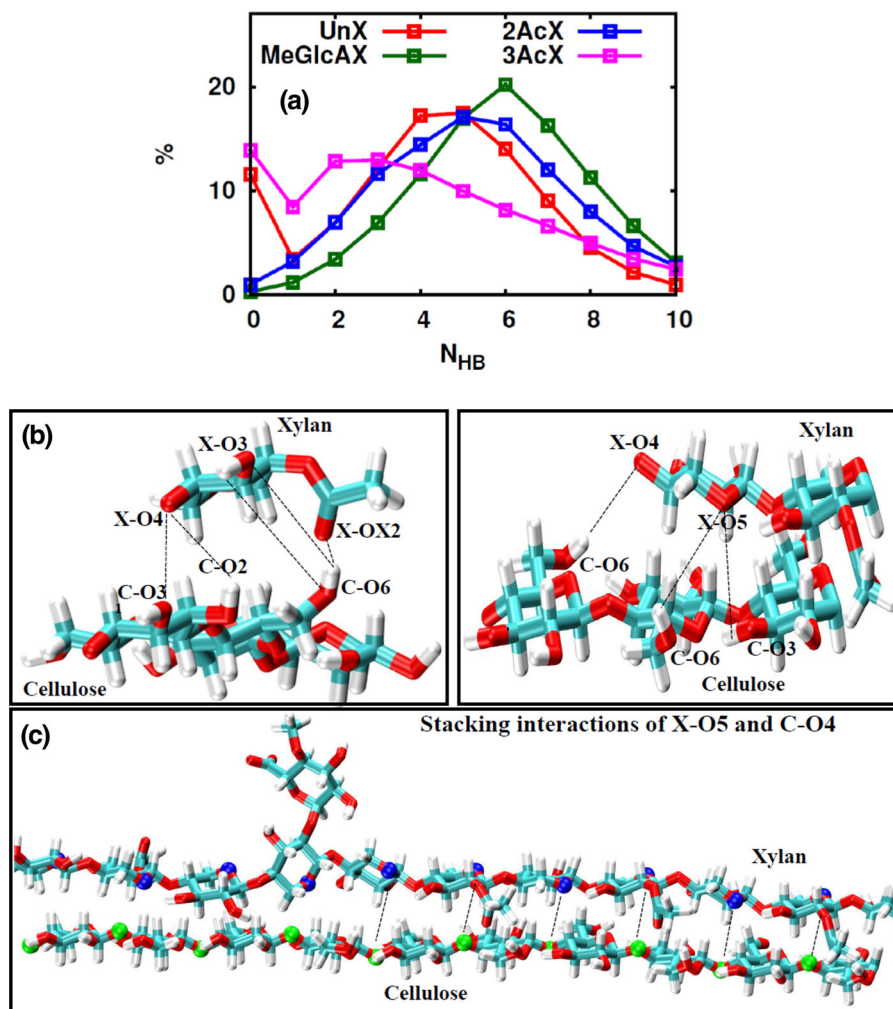
Fig. 8 a Percentage of xylan conformations forming different numbers of xylan-cellulose hydrogen bonds. **b** Snapshot of different atoms involved in hydrogen bonding interactions in xylan and cellulose, both X-O3 and C-O6 can act as both donors and acceptors. **c** Stacking interactions between X-O5 and C-O4. X-O5 and C-O4 are depicted in blue and green colors, respectively

restricted dihedral angles and is conformationally more rigid in the presence of cellulose than the other xylans. These findings are consistent with previous simulations showing that steric interactions between α-1,2 GlcA or α-1,2 Ara substitutions with xylan backbone restrict the allowed range of glycosidic bonds on the cellulose surface, while α-1,3 GlcA and α-1,3 Ara do not (Martínez-Abad et al. 2017; Pereira et al. 2017). Regioselectivity of the acetyl substitutions at O-2 and O-3 has been shown to influence the backbone flexibility of xylans in aqueous solution (Berglund et al. 2020). It can thus be concluded that O-2 substitutions in the xylan backbone result in more

rigid twofold xylan conformation in the presence of cellulose, irrespective of the nature the substituent (Ara/GlcA/Ac).

The xylan conformations can be distinguished as twofold or threefold helical screw by computing the sum of dihedral angles, $\phi + \Psi$, at a particular glycosidic oxygen (Mazeau et al. 2005; French and Johnson 2009). A value of $\phi + \Psi = 120°$ indicates a twofold helical screw conformation, whereas $\phi + \Psi = 190°$ represent a left-handed threefold (Mazeau et al. 2005; French and Johnson 2009). Right-handed threefold conformations ($\phi + \Psi = 50°$) do not exist in nature. In the absence of
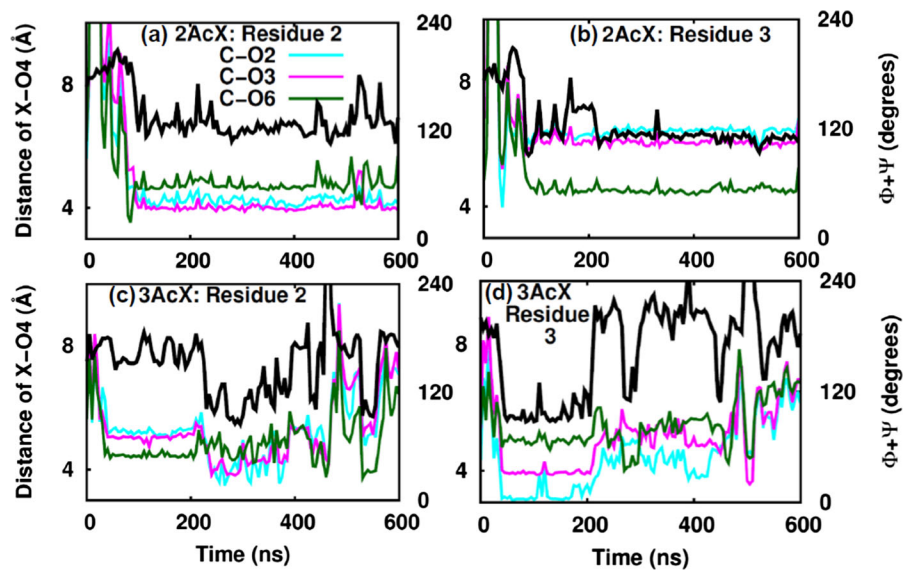
Fig. 9 Distance of glycosidic O4 of xylosyl residues (X-O4) from cellulose surface for (**a–b**) 2AcX, and (**c–d**) 3AcX conformations. These plots show the cumulative average of these distances as a function of time. The black line represents the sum of dihedral conformations as denoted on y2 axis

Fig. 10 Distance of glycosidic O5 of xylosyl residues (X-O5) from cellulose surface for (**a–b**) 2AcX, and (**c–d**) 3AcX conformations. These plots show the cumulative average of these distances as a function of time. The black line represents the sum of dihedral conformations as denoted on y2 axis
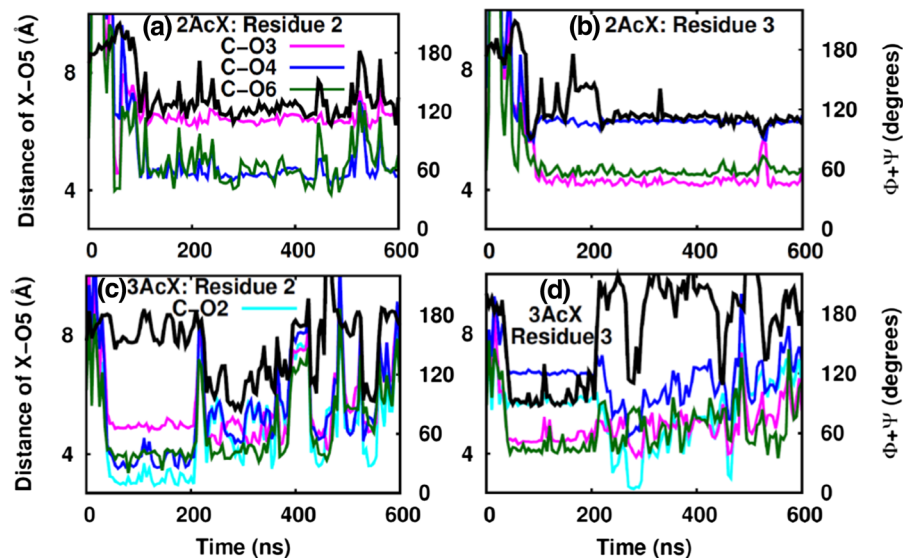
cellulose, the histograms for the sum of dihedral angles ($\phi + \Psi$), averaged over all residues, show an even distribution centered around $\phi + \Psi = 190°$ (Fig. 5), indicating that all four xylans predominantly adopt threefold helical screw conformations in the absence of cellulose. The time-evolution plots show

that the threefold helical screw conformation is stable throughout the entire trajectories (Fig. S1). Thus, xylan maintains threefold helical screw conformations in a cellulose-deficient environment independent of the chemical nature and position of the substitution.
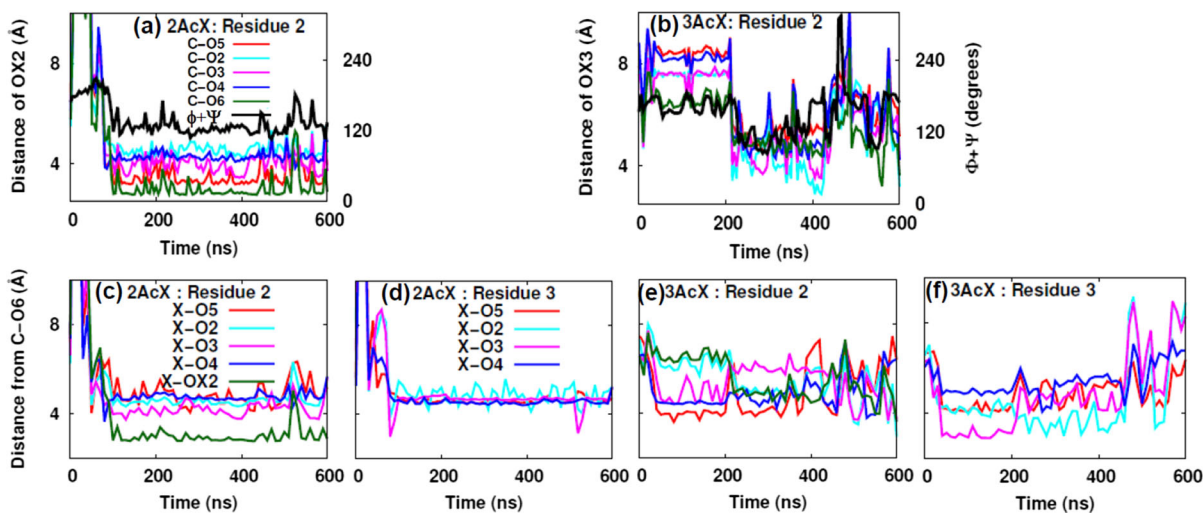
Fig. 11 Distance from cellulose oxygens of (**a**) OX2 of 2AcX, and (**b**) OX3 of 3AcX. The black line represents the helical screw conformations as denoted on y2 axis. Distance of O6 of cellulose (C-O6) from different oxygens in xylosyl residues of (**c–d**) 2AcX and (**e–f**) 3AcX conformations. These plots show the cumulative average of these distances as a function of time

Table 1 Average values for the radius of gyration (R_g) and root mean square fluctuations (RMSF) for xylan conformations in the absence and presence of cellulose

		R_g (Å)	RMSF (Å)
Absence of cellulose	UnX	12.7 (0.2)	0.2 (0)
	MeGlcAX	12.4 (0.1)	0.3 (0)
	2AcX	12.8 (0.3)	0.4 (0)
	3AcX	12.8 (0.1)	0.3 (0)
Presence of cellulose	UnX	13.0 (0.5)	0.2 (0)
	MeGlcAX	12.7 (0.7)	0.2 (0)
	2AcX	13.2 (0.8)	0.4 (0.1)
	3AcX	12.9 (0.4)	0.3 (0)

The values are averaged over time and the four simulations for each system. The values in the parentheses denote standard error

In the presence of cellulose, all residues of UnX continue to maintain a threefold helical screw conformation (Figs. 6a and S2a). Similar to UnX, the unsubstituted residues 2 to 6 of MeGlcAX also maintain a threefold helical screw conformation (Figs. 6b and S2b). This is consistent with previous MD studies (Falcoz-Vigne et al. 2017) where bare xylan in the absence of any restraints adsorbs in threefold helical screw conformations on the cellulose surface. Interestingly, the histograms around the MeGlcA substituted residue 8 show a major peak at

$\phi + \Psi = 190°$ and a minor peak at $\phi + \Psi = 85° - 95°$ (Figs. 6c–d, S2c–d), indicating that the majority of the residues maintain threefold helical screw conformations while sometimes adopting twofold helical conformations. It can thus be surmised that one MeGlcA substitution per 11 residues is not enough to preserve the twofold helical conformations.

For 2AcX, the histograms for $\phi + \Psi$ for residues 2 to 6 show a bimodal distribution with peaks around $\phi + \Psi = \sim 100°-130°$ and $\phi + \Psi = 190°$ (Figs. 6e–i). The majority of the conformations are twofold helical screw. It is noted that the twofold conformation is most dominant for residue 4, the only residue flanked by Ac substituted residues (2 and 6) on both sides. Residues 2 to 6 show a switch to twofold conformations around 100 ns, which is then maintained over the remaining simulation (Fig. S2). The MeGlcA substituted residue 8 and the residues in its vicinity adopt mainly a threefold conformation (for both 2AcX, Figs. 6j-l and MeGlcAX, Figs. 6c-d). We speculate that residues 7–10 do not show substantial population of twofold helix as this part of the xylan backbone is not periodically substituted by Ac groups. Periodic Ac substitution on a xylan chain of larger DP may stabilize the twofold helical screw conformation at each glycosidic linkage.

For 3AcX, although the distribution of $\phi + \Psi$ also shows two distinct peaks around $\sim 180°-190°$ and $\sim 90°-95°$ (Figs. 6m-o,q,s) the majority of the

populations is in the threefold helical screw conformation. Residues 2 to 4 have relatively more twofold conformations than the other residues. Similar to 2AcX and MeGlcAX a threefold conformation is observed around the MeGlcA substituted residue 8. Visual inspection of the simulations shows that MeGlcA is oriented away from the cellulose surface during the entire simulation run and this orientation is unaffected by any changes in the topological environment around the MeGlcA substituted residue. This is consistent with previous studies where MeGlcA substituted residue was observed to have a low affinity for the.

cellulose (Linder et al. 2003; Martínez-Abad et al. 2017).

Scatter plots of $\phi + \Psi$ of representative xylosyl residues and their distances from the cellulose surface show that the majority of the twofold helical conformations for 2AcX and 3AcX are found mostly within 3–5 Å from the cellulose surface, indicating stable xylan-cellulose binding (Fig. 7). When the xylosyl residues are located at distances > 15 Å from the cellulose surface, they adopt predominantly threefold helical screw conformations. Visual inspection of the simulations showed that none of the 2AcX conformations detach from the cellulose surface, unlike UnX and 3AcX (Figs. 3d-f). Also, in some MeGlcAX conformations the residues around the MeGlcA substituted residue (7 to 9) anchor to cellulose surface while other residues orient away from the cellulose surface. Thus, xylan-cellulose interactions promote and stabilize the twofold helical screw xylan conformations, while threefold conformations correspond to stretched xylan conformations interacting preferably with water rather than cellulose.

To understand how 2AcX conformations interact with the cellulose surface, we first computed the number of intermolecular contacts, N_c, between xylan and cellulose (Table 2). N_c is statistically similar between all 4 forms of xylan, although N_c tends to be larger for MeGlcAX and 2AcX than for UnX and 3AcX. Decomposing N_c into contributions from the unsubstituted, Ac substituted and MeGlcA substituted residues (Table 2) shows that the number of contacts per unsubstituted residue is maximal for 2AcX. The Ac bearing residues form more contacts with cellulose for 2AcX than for 3AcX. The fraction of xylosyl residues that is bound to the cellulose surface is only 38% for UnX, while it is $\sim$ 65–71% for MeGlcAX,

2AcX, and 3AcX (Table 2). This suggests that substitution on the xylan backbone promotes the association of xylan with cellulose. Hence, N_c, is not correlated with the formation of twofold helical screw conformation, but 2AcX interacts most effectively with cellulose by forming maximum number of contacts both via its unsubstituted and substituted residues (Table 2).

UnX and 3AcX form on average form $\sim$ 4 hydrogen bonds with cellulose while MeGlcAX and 2AcX form 7 and 5 hydrogen bonds, respectively (Table 2). UnX and 3AcX have a higher probability of forming 0–3 hydrogen bonds, while MeGlcAX and 2AcX form more frequently 6–10 hydrogen bonds (Fig. 8a). The unsubstituted residues of both 2AcX and 3AcX conformations are involved in 2–3 hydrogen bonds with the cellulose surface (Table 2). Interestingly, the acetylated residues in 2AcX form $\sim$ 2 hydrogen bonds while for 3AcX form $\sim$ 1 hydrogen bond, thus hydrogen bond patterns do not match the inter-atomic contacts. The residue bearing the MeGlcA group consistently forms on average one hydrogen bond with the cellulose surface for all xylan decorations. This is consistent with a previous MD study where bare xylan was observed to have the weakest interactions with (1–10) hydrophilic and (200) hydrophobic surfaces followed by xylan substituted with one MeGlcA group (Martínez-Abad et al. 2017).

UnX, MeGlcAX and 3AcX occasionally form $\sim$ 1 intra-molecular hydrogen bond. While 2AcX forms $\sim$ 2 intra-molecular hydrogen bonds. The hydrogen bonding interactions in 2AcX are dominated by X-O3 which acts as donor while X-O2 and X-O5 of adjacent xylan residues act as acceptors. X-O3 also forms hydrogen bonds with acetylated oxygen (X-OX2) of the same or adjacent residues in 2AcX. Since X-O3 is substituted by acetyl residues in 3AcX conformations, the hydrogen bonding is no longer dominated only by X-O3. In 3AcX, both X-O2 and X-O3 act as donors and acceptors. Thus, it can be concluded that intra-molecular H-bonds involving X-O3 of the xylan backbone primarily influence the stability of the twofold helical screw conformations on the cellulose surface.

The increase in percentage of bound conformations does not directly correlate to the switch from threefold to twofold helical screw conformations on the cellulose surface. The reasons for this will now be discussed. To determine which specific cellulose-

Table 2 Order parameters for xylan conformations in the presence of cellulose

		UnX	MeGlcAX	2AcX	3AcX
$N_{contacts}$	All residues	153 (52)	225 (10)	229 (36)	172 (15)
	Per unsubstituted residue	14 (5)	23 (1)	26 (2)	21 (3)
	MeGlcA residue	–	38 (11)	25 (7)	14 (2)
	Per Ac residue	–	–	27 (5)	22 (1)
% of bound conformations	$N_{contacts} > 15$ per residue	37.8 (13.4)	65.5 (2.7)	70.7 (11.1)	67.5 (7.3)
N_{HB}	All residues	4 (1)	7 (1)	5 (0)	3 (0)
	Unsubstituted residues	–	–	3 (1)	2 (1)
	Ac residues	–	–	2 (0)	1 (0)

We define the xylan conformations as bound if each xylosyl residue forms at least 15 contacts with the cellulose surface. Data are averaged over t > 400 ns and the four simulations for each system. The values in the parentheses denote standard error

xylan interactions stabilize the twofold helical screw conformations, we computed the distances between xylan glycosidic (backbone) oxygen atoms X-O4 and X-O5 and the cellulose surface oxygen atoms (Figs. 8b, 9 and 10, respectively). The time-dependence of the distance between the X-O4 of substituted xylan residues and cellulose C-O2 or C-O3 roughly follows the time dependence of $\phi + \Psi$ (Figs. 9, S2). Correspondingly, the distance between X-O4 of the unsubstituted xylan residues and the cellulose C-O6 follows the $\phi + \Psi$ time dependence. Transitions from twofold to threefold helical screw conformations are observed roughly at similar time domains when these atoms are in proximity. When in a twofold screw conformation the oxygen X-O5 of substituted residues interacts mostly with C-O6 and C-O4 (Figs. 10, S3) while X-O5 interacts with C-O6 and C-O3 for the unsubstituted residues for 2AcX. X-O5 and C-O4 stack to stabilize xylan-cellulose interactions while all the other O–O interactions are hydrogen bonding interactions (Fig. 8c).

Interestingly, the acetylated oxygen, OX2 of the substituted residues 2, 4, and 6 of 2AcX (Figs. 8b, 11a, S4) interacts with all the oxygens of cellulose (distance < 5 Å), but C-O6 is closest. OX2 of non-periodic acetylated residue 10 in 2AcX is further away from the cellulose surface (Fig. S4d). Also, C-O6 has favorable interactions with X-O3 of 2AcX (Figs. 8b,11c-d). These interactions are missing for 3AcX conformations due to substitution at X-O3 of xylan backbone. It can thus be concluded that the interaction of OX2 and X-O3 of acetylated residues with C-O6 is a specific interaction that facilitates the

formation of twofold conformations for 2AcX. Similarly, the twofold helical screw conformation for 3AcX is maintained as long as OX3 is proximal to C-O6 and has a role in stabilizing xylan-cellulose interactions. These results are in agreement with a previous MD study of docked acetylated xylan in twofold conformation on (010) and (020) hydrophilic surfaces where O6 of cellulose was observed to play a central role in stabilizing cellulose-xylan interactions (Busse-Wicher et al. 2014). Similarly, the orientation of Ara substituents towards the cellulose surface result in stronger interactions of xylan with the cellulose surface than when the side chains orient away from the surface (Martínez-Abad et al. 2017).

Our study is consistent with previous studies showing that the presence of substitutions at alternate positions stabilizes the cellulose-xylan interactions by favoring twofold helical screw conformations for xylan (Bromley et al. 2013; Busse-Wicher et al. 2014, 2016; Simmons et al. 2016; Pereira et al. 2017). Previous computational work has found unsubstituted UnX to form twofold helical screw on hydrophilic cellulose surfaces (Busse-Wicher et al. 2014; Falcoz-Vigne et al. 2017; Martínez-Abad et al. 2017). In those studies, the glycosidic bonds of UnX were restrained to a twofold conformation for part of the MD simulation or the simulations started with xylan tightly docked to cellulose. The unrestrained MD presented here, in which xylan is initially away from the cellulose, show a switch in the helical fold after ∼ 100 ns, which suggests that long simulations (> ∼ 100 ns) are probably needed to detect substantial change in the xylan conformations. Some

experimental studies elucidated that the increase in the number of substitutions on the xylan backbone reduces the propensity for adsorption on the cellulose surface (Kabel et al. 2007; Bosmans et al. 2014). The degree of acetylation of such xylan was 0.7 and the effects were much more pronounced for Ara substitutions as compared to Ac groups (Kabel et al. 2007). It can thus be speculated that a higher degree of substitution (> 50%) may reduce adsorption on cellulose surface due to the unavailability of enough unsubstituted residues for interaction with cellulose, but future MD studies are required to test this hypothesis.

Conclusions

We report here an investigation using unrestrained MD simulations of the switch of xylans with different decorations from threefold helical screw conformations, found in cellulose-deficient environments, to twofold helical screw in the presence of cellulose. In the absence of cellulose, all xylans show comparable behavior and adopt a threefold helical screw conformation. Bare UnX xylans maintain threefold helical screw conformations even in the presence of cellulose and occasionally detach from cellulose surface, illustrating that bare xylan interacts weakly with the cellulose surface.

2 Ac substituted xylan is conformationally rigid with restricted glycosidic dihedral angles resulting in the formation of a twofold helical screw conformation on the surface of cellulose. These conformations strongly associate with (110) hydrophilic cellulose surface. The hydrogen-bonding interactions of C-O6 of cellulose with xylan oxygens X-O3, X-O4, X-O5 and the acetylated oxygen X-OX2 play a central role in stabilizing the twofold helical screw conformations for 2AcX conformations. 3 Ac substituted xylan assumes predominantly threefold conformations and has dynamic interactions with cellulose, occasionally showing a transition to twofold helical screw when side-chain acetyl (X-OX3) or glycosidic dihedral angle oxygens (X-O4, X-O5) interact closely with the cellulose surface. Xylans with only one MeGlcA decoration also form a comparable number of xylan-cellulose contacts as that of 2AcX conformations but do not adopt twofold helical screw conformations, illustrating that many xylan decorations are needed in sustaining twofold helical screw xylan conformations.

Thus, the higher number of contacts between xylan and cellulose surface is not correlated with the formation of twofold helical screw conformations as only specific O–O contacts with the cellulose surface by both substituted and unsubstituted residues of xylan trigger the formation of rigid twofold helical screw conformations. Combining our results with a previous study on the role of O-2 Ara and GlcA xylan decorations on cellulose-xylan interactions (Pereira et al. 2017) demonstrates that, independent of the chemical nature of the substituent, O-2 substitutions play a dominant role in promoting cellulose-xylan interactions and formation of the twofold helical screw xylan, provided that the substitutions follow a periodic pattern. These insights improve our current understanding of the molecular underpinnings of plant cell wall architecture.

Compliance with ethical standards

Conflicts of interest There are no conflicts to declare.

References

Abraham MJ, Murtola T, Schulz R et al (2015) Gromacs: high performance molecular simulations through multi-level parallelism from laptops to supercomputers. SoftwareX 1–2:19–25. https://doi.org/10.1016/j.softx.2015.06.001

Almond A, Sheenan JK (2003) Predicting the molecular shape of polysaccharides from dynamic interactions with water. Glycobiology 13:255–264. https://doi.org/10.1093/glycob/cwg031

Bergenstråhle M, Wohlert J, Larsson PT et al (2008) Dynamics of cellulose−water interfaces: NMR spin−lattice relaxation times calculated from atomistic computer simulations. J Phys Chem B 112:2590–2595

Berglund J, Angles d'Ortoli T, Vilaplana F et al (2016) A molecular dynamics study of the effect of glycosidic linkage type in the hemicellulose backbone on the molecular chain flexibility. Plant J 88:56–70. https://doi.org/10.1111/tpj.13259

Berglund J, Kishani S, Morais de Carvalho D et al (2020) Acetylation and sugar composition influence the (in)solubility of plant β-mannans and their interaction with cellulose surfaces. ACS Sustain Chem Eng 8:10027–10040. https://doi.org/10.1021/acssuschemeng.0c01716

Biely P, Mackenzie CR (1986) Cooperativity of esterases and xylanases in the enzymatic degradation of acetyl xylan. Nat Biotechnol 4:731–733. https://doi.org/10.1038/nbt0886-731

Bischoff V, Nita S, Neumetzler L et al (2010) TRICHOME BIREFRINGENCE and its homolog AT5G01360 encode plant-specific DUF231 proteins required for cellulose biosynthesis in arabidopsis. Plant Physiol 153:590–602. https://doi.org/10.1104/pp.110.153320

Bosmans TJ, Stépán AM, Toriz G et al (2014) Assembly of debranched xylan from solution and on nanocellulosic surfaces. Biomacromol 15:924–930. https://doi.org/10.1021/bm4017868

Bromley JR, Busse-Wicher M, Tryfona T et al (2013) GUX1 and GUX2 glucuronyltransferases decorate distinct domains of glucuronoxylan with different substitution patterns. Plant J 74:423–434. https://doi.org/10.1111/tpj.12135

Brown DM, Goubet F, Wong VW et al (2007) Comparison of five xylan synthesis mutants reveals new insight into the mechanisms of xylan synthesis. Plant J 52:1154–1168. https://doi.org/10.1111/j.1365-313X.2007.03307.x

Busse-Wicher M, Gomes TCF, Tryfona T et al (2014) The pattern of xylan acetylation suggests xylan may interact with cellulose microfibrils as a twofold helical screw in the secondary plant cell wall of Arabidopsis thaliana. Plant J 79:492–506. https://doi.org/10.1111/tpj.12575

Busse-Wicher M, Li A, Silveira RL et al (2016) Evolution of xylan substitution patterns in gymnosperms and angiosperms: implications for xylan interaction with cellulose. Plant Physiol 171:2418–2431. https://doi.org/10.1104/pp.16.00539

Bussi G, Donadio D, Parrinello M (2007) Canonical sampling through velocity rescaling. J Chem Phys 126:014101. https://doi.org/10.1063/1.2408420

Carroll A, Somerville C (2009) Cellulosic biofuels. Annu Rev Plant Biol 60:165–182. https://doi.org/10.1146/annurev.arplant.043008.092125

Chong SL, Virkki L, Maaheimo H et al (2014) O-Acetylation of glucuronoxylan in arabidopsis thaliana wild type and its change in xylan biosynthesis mutants. Glycobiology 24:494–506. https://doi.org/10.1093/glycob/cwu017

Chundawat SPS, Beckham GT, Himmel ME, Dale BE (2011) Deconstruction of lignocellulosic biomass to fuels and chemicals. Annu Rev Chem Biomol Eng 2:121–145. https://doi.org/10.1146/annurev-chembioeng-061010-114205

Cosgrove D (2014) Re-constructing our models of cellulose and primary cell wall assembly. Curr Opin Plant Biol 22:122–131

Cosgrove DJ, Jarvis MC (2012) Comparative structure and biomechanics of plant primary and secondary cell walls. Plant Sci, Front. https://doi.org/10.3389/fpls.2012.00204

Darden T, York D, Pedersen L (1993) Particle mesh Ewald: an N·log(N) method for Ewald sums in large systems. J Chem Phys 98:10089–10092. https://doi.org/10.1063/1.464397

de Carvalho DM, Berglund J, Marchand C et al (2019) Improving the thermal stability of different types of xylan by acetylation. Carbohydr Polym 220:132–140. https://doi.org/10.1016/j.carbpol.2019.05.063

Ebringerova A, Heinze T (2000) Xylan and xylan derivatives – biopolymers with valuable properties, 1. Naturally occurring xylans structures, isolation procedures and properties. Macromol Rapid Commun 21:869–883. https://doi.org/10.1002/1521-3927

Evtuguin DV, Tomás JL, Silva AMS, Neto CP (2003) Characterization of an acetylated heteroxylan from Eucalyptus globulus Labill. Carbohydr Res 338:597–604. https://doi.org/10.1016/S0008-6215(02)00529-3

Falcoz-Vigne L, Ogawa Y, Molina-Boisseau S et al (2017) Quantification of a tightly adsorbed monolayer of xylan on cellulose surface. Cellulose 24:3725–3739. https://doi.org/10.1007/s10570-017-1401-z

French AD, Johnson GP (2009) Cellulose and the twofold screw axis: modeling and experimental arguments. Cellulose 16:959–973. https://doi.org/10.1007/s10570-009-9347-4

Gao Y, He C, Zhang D et al (2017) Two trichome birefringence-like proteins mediate xylan acetylation, which is essential for leaf blight resistance in rice. Plant Physiol 173:470–481. https://doi.org/10.1104/pp.16.01618

Gomes TCF, Skaf MS (2012) Cellulose-builder: a toolkit for building crystalline structures of cellulose. J Comput Chem 33:1338–1346. https://doi.org/10.1002/jcc.22959

Grantham NJ, Wurman-Rodrich J, Terrett OM et al (2017) An even pattern of xylan substitution is critical for interaction with cellulose in plant cell walls. Nat Plants 3:859–865. https://doi.org/10.1038/s41477-017-0030-8

Guvench O, Hatcher E, Venable RM et al (2009) CHARMM additive all-atom force field for glycosidic linkages between hexopyranoses. J Chem Theory Comput 5:2353–2370. https://doi.org/10.1021/ct900242e

Hess B (2008) P-LINCS: a parallel linear constraint solver for molecular simulation. J Chem Theory Comput 4:116–122. https://doi.org/10.1021/ct700200b

Hess B, Bekker H, Berendsen HJC, Fraaije JGEM (1997) LINCS: a linear constraint solver for molecular

simulations. J Comput Chem 18:1463–1472. https://doi.org/10.1002/(SICI)1096-987X(199709)18:12%3c1463::AID-JCC4%3e3.0.CO;2-H

Himmel ME, Ding S, Johnson DK, Adney WS (2007) Biomass recalcitrance: engineering plants and enzymes for biofuels production. Science 315:804–808s

Humphrey W, Dalke A, Schulten K (1996) VMD: visual molecular dynamics. J Mol Graph 14:33–38. https://doi.org/10.1016/0263-7855(96)00018-5

Jaafar Z, Mazeau K, Boissière A et al (2019) Meaning of xylan acetylation on xylan-cellulose interactions: a quartz crystal microbalance with dissipation (QCM-D) and molecular dynamic study. Carbohydr Polym 226:115315. https://doi.org/10.1016/j.carbpol.2019.115315

Jo S, Kim T, Iver V, Im W (2008) CHARMM-GUI: a web-based graphical user interface for CHARMM. J Comput Chem 29:1859–1865

Jo S, Song KC, Desaire H et al (2011) Glycan reader: Automated sugar identification and simulation preparation for carbohydrates and glycoproteins. J Comput Chem 32:3135–3141. https://doi.org/10.1002/jcc.21886

Johnson AM, Kim H, Ralph J, Mansfield SD (2017) Natural acetylation impacts carbohydrate recovery during deconstruction of Populus trichocarpa wood. Biotechnol Biofuels 10:1–12. https://doi.org/10.1186/s13068-017-0734-z

Jorgensen WL, Chandrasekhar J, Madura JD et al (1983) Comparison of simple potential functions for simulating liquid water comparison of simple potential functions for simulating liquid water. J Chem Phys 79:926. https://doi.org/10.1063/1.445869

Kabel MA, van den Borne H, Vincken JP et al (2007) Structural differences of xylans affect their interaction with cellulose. Carbohydr Polym 69:94–105. https://doi.org/10.1016/j.carbpol.2006.09.006

Kang X, Kirui A, Dickwella Widanage MC et al (2019) Lignin-polysaccharide interactions in plant secondary cell walls revealed by solid-state NMR. Nat Commun 10:347. https://doi.org/10.1038/s41467-018-08252-0

Koutaniemi S, Guillon F, Tranquet O et al (2012) Substituent-specific antibody against glucuronoxylan reveals close association of glucuronic acid and acetyl substituents and distinct labeling patterns in tree species. Planta 236:739–751. https://doi.org/10.1007/s00425-012-1653-7

Kubicki JD, Yang H, Sawada D et al (2018) The shape of native plant cellulose microfibrils. Sci Rep 8:13983. https://doi.org/10.1038/s41598-018-32211-w

Kumar R, Bhagia S, Smith MD et al (2018) Cellulose-hemicellulose interactions at elevated temperatures increase cellulose recalcitrance to biological conversion. Green Chem 20:921–934. https://doi.org/10.1039/c7gc03518g

Larsson PT (2003) Interaction between cellulose I and hemicelluloses studied by spectral fitting of CP/MAS 13C-NMR spectra. ACS Symp Ser Hemicelluloses Sci Technol 864:254–268

Larsson PT, Hult EL, Wickholm K et al (1999) CP/MAS 13C-NMR spectroscopy applied to structure and interaction studies on cellulose I. Solid State Nucl Magn Reson 15:31–40. https://doi.org/10.1016/S0926-2040(99)00044-2

Linder A, Bergman R, Bodin A, Gatenholm P (2003) Mechanism of assembly of xylan onto cellulose surfaces. Langmuir 19:5072–5077. https://doi.org/10.1021/la0341355

Ling Z, Edwards JV, Nam S et al (2020) Conformational analysis of xylobiose by DFT quantum mechanics. Cellulose 27:1207–1224. https://doi.org/10.1007/s10570-019-02874-3

Lunin V, Wang H-T, Bharadwaj V et al (2020) Molecular mechanism of polysaccharide acetylation by the Arabidopsis xylan O-acetyltransferase XOAT1. Plant Cell 32:2367–2382. https://doi.org/10.1105/tpc.20.00028

Luzar A (2000) Resolving the hydrogen bond dynamics conundrum. J Chem Phys 113:10663–10675. https://doi.org/10.1063/1.1320826

Martínez-Abad A, Berglund J, Toriz G et al (2017) Regular motifs in xylan modulate molecular flexibility and interactions with cellulose surfaces. Plant Physiol 175:1579–1592. https://doi.org/10.1104/pp.17.01184

Martínez-abad A, Jiménez-quero A (2020) Influence of the molecular motifs of mannan and xylan populations on their recalcitrance and organization in spruce softwoods. Green Chem 22:3956–3970. https://doi.org/10.1039/d0gc01207f

Mazeau K, Moine C, Krausz P, Gloaguen V (2005) Conformational analysis of xylan chains. Carbohydr Res 340:2752–2760. https://doi.org/10.1016/j.carres.2005.09.023

Meng X, Ragauskas AJ (2014) Recent advances in understanding the role of cellulose accessibility in enzymatic hydrolysis of lignocellulosic substrates. Curr Opin Biotechnol 27:150–158. https://doi.org/10.1016/j.copbio.2014.01.014

Mikkelsen D, Flanagan BM, Wilson SM et al (2015) Interactions of arabinoxylan and (1,3)(1,4)-β-glucan with cellulose networks. Biomacromol 16:1232–1239. https://doi.org/10.1021/acs.biomac.5b00009

Mortimer JC, Miles GP, Brown DM et al (2010) Absence of branches from xylan in Arabidopsis gux mutants reveals potential for simplification of lignocellulosic biomass. Proc Nat Acad Sci USA 107:17409–17414. https://doi.org/10.1073/pnas.1005456107

Nieduszynski A, Marchessault H (1972) Structure of beta, D (1–4')-Xylan Hydrate. Biopolymers 11:1335–1344

Nishiyama Y, Langan P, Chanzy H (2002) Crystal structure and hydrogen-bonding system in cellulose Iβ from synchrotron X-ray and neutron fiber diffraction. J Am Chem Soc 124:9074–9082. https://doi.org/10.1021/ja0257319

Park SJ, Lee J, Patel DS et al (2017) Glycan reader is improved to recognize most sugar types and chemical modifications in the protein data bank. Bioinformatics 33:3051–3057. https://doi.org/10.1093/bioinformatics/btx358

Park SJ, Lee J, Qi Y et al (2019) CHARMM-GUI Glycan Modeler for modeling and simulation of carbohydrates and glycoconjugates. Glycobiology 29:320–331. https://doi.org/10.1093/glycob/cwz003

Parrinello M, Rahman A (1981) Polymorphic transitions in single crystals: A new molecular dynamics method. J Appl Phys 52:7182–7190. https://doi.org/10.1063/1.328693

Pauly M, Keegstra K (2010) Plant cell wall polymers as precursors for biofuels. Curr Opin Plant Biol 13:304–311. https://doi.org/10.1016/j.pbi.2009.12.009

Pawar PMA, Koutaniemi S, Tenkanen M, Mellerowicz EJ (2013) Acetylation of woody lignocellulose: significance and regulation. Front Plant Sci 4:1–8. https://doi.org/10.3389/fpls.2013.00118

Pereira CS, Silveira RL, Dupree P, Skaf MS (2017) Effects of xylan side-chain substitutions on xylan-cellulose interactions and implications for thermal pretreatment of cellulosic biomass. Biomacromol 18:1311–1321. https://doi.org/10.1021/acs.biomac.7b00067

Qaseem MF, Wu AM (2020) Balanced xylan acetylation is the key regulator of plant growth and development, and cell wall structure and for industrial utilization. Int J Mol Sci 21:7875. https://doi.org/10.3390/ijms21217875

Van RR, Nieves IU, Shanmugam KT et al (2018) Techno-economic evaluation of cellulosic ethanol production based on pilot biorefinery data: a case study of sweet sorghum bagasse processed via L + SScF. Bioenergy Res 11:414–425

Scheller HV, Ulvskov P (2010) Hemicelluloses. Annu Rev Plant Biol 61:263–289. https://doi.org/10.1146/annurev-arplant-042809-112315

Shrestha UR, Smith S, Pingali SV et al (2019) Arabinose substitution effect on xylan rigidity and self-aggregation. Cellulose 26:2267–2278. https://doi.org/10.1007/s10570-018-2202-8

Simmons TJ, Mortimer JC, Bernardinelli OD et al (2016) Folding of xylan onto cellulose fibrils in plant cell walls revealed by solid-state NMR. Nat Commun 7:13902. https://doi.org/10.1038/ncomms13902

Song B, Zhao S, Shen W et al (2020) Direct measurement of plant cellulose microfibril and bundles in native cell walls. Front Plant Sci 11:1–11. https://doi.org/10.3389/fpls.2020.00479

Tarasov D, Leitch M, Fatehi P (2018) Lignin-carbohydrate complexes: properties, applications, analyses, and methods of extraction: a review. Biotechnol Biofuels 11:269. https://doi.org/10.1186/s13068-018-1262-1

Teleman A, Tenkanen M, Jacobs A, Dahlman O (2002) Characterization of O-acetyl-(4-O-methylglucurono)xylan isolated from birch and beech. Carbohydr Res 337:373–377. https://doi.org/10.1016/S0008-6215(01)00327-5

Thomas LH, Forsyth VT, Adriana Š et al (2013) Structure of cellulose microfibrils in primary cell walls from collenchyma. Plant Physiol 161:465–476. https://doi.org/10.1104/pp.112.206359

Torshin IY, Weber IT, Harrison RW (2002) Geometric criteria of hydrogen bonds in proteins and identification of "bifurcated" hydrogen bonds. Protein Eng 15:359–363. https://doi.org/10.1093/protein/15.5.359

Westbye P, Svanberg C, Gatenholm P (2006) The effect of molecular composition of xylan extracted from birch on its assembly onto bleached softwood kraft pulp. Holzforschung 60:143–148. https://doi.org/10.1515/HF.2006.023

Xiong G, Cheng K, Pauly M (2013) Xylan O-acetylation impacts xylem development and enzymatic recalcitrance as indicated by the arabidopsis mutant tbl29. Mol Plant 6:1373–1375. https://doi.org/10.1093/mp/sst014

Xiong G, Dama M, Pauly M (2015) Glucuronic Acid Moieties on Xylan Are Functionally Equivalent to O-Acetyl-Substituents. Mol Plant 8:1119–1121. https://doi.org/10.1016/j.molp.2015.02.013

Zhang B, Zhang L, Li F et al (2017) Control of secondary cell wall patterning involves xylan deacetylation by a GDSL esterase. Nat Plants 3:1–9. https://doi.org/10.1038/nplants.2017.17

Zhao Z, Crespi VH, Kubicki JD et al (2014) Molecular dynamics simulation study of xyloglucan adsorption on cellulose surfaces: effects of surface hydrophobicity and side-chain variation. Cellulose 21:1025–1039. https://doi.org/10.1007/s10570-013-0041-1

Springer